Disturbances from Shock/Boundary Layer Interactions Affecting Upstream Hypersonic Flow

AIAA Paper 2005-4897, Presented at the 35th Fluid Dynamics Conference, Toronto, Canada, Jun. 2005

Craig R. Skoch*, Steven P. Schneider†, and Matthew P. Borg‡
School of Aeronautics and Astronautics
Purdue University
West Lafayette, IN 47907-1282

ABSTRACT

Laminar-turbulent transition is critical for vehicles which fly at hypersonic speeds for extended periods. To improve on existing correlations, prediction methods that incorporate knowledge of the transition mechanisms are necessary and now feasible. Purdue continues to develop the Boeing/AFOSR Mach-6 Tunnel to seek quiet flow at high Reynolds numbers, with noise levels comparable to flight. It has been shown previously that quiet flow is only possible at low stagnation pressures probably because a separation bubble develops on the bleed lip. A new upstream portion of the nozzle was built without the high polish, and was found to increase the quiet-flow stagnation pressure from 8 psia to 20 psia. When laminar boundary layers are maintained on the walls of the nozzle, the flow becomes separated about two-thirds of the distance down the nozzle. It is shown here that this separation is caused by shocks from the sting mount in the diffuser that disturb the boundary layer far upstream. Attempts have been made to try to prevent these disturbances from traveling so far upstream, but have met with little success. This limits the ability to test models using the quiet flow.

*Research Assistant. Student Member, AIAA.
†Professor. Associate Fellow, AIAA.
‡Research Assistant. Student Member, AIAA.

INTRODUCTION

Hypersonic Laminar-Turbulent Transition

Laminar-turbulent transition in hypersonic boundary layers is important for prediction and control of heat transfer, skin friction, and other boundary layer properties. Vehicles that spend extended periods at hypersonic speeds may be critically affected by the uncertainties in transition prediction, depending on their Reynolds numbers. However, the mechanisms leading to transition are still poorly understood, even in low-noise environments.

Many transition experiments have been carried out in conventional ground-testing facilities over the past 50 years.[1] However, these experiments are contaminated by the high levels of noise that radiate from the turbulent boundary layers normally present on the wind tunnel walls.[2] These noise levels, typically 0.5-1% of the mean, are an order of magnitude larger than those observed in flight[3,4] and can cause transition to occur an order of magnitude earlier than in flight.[2,4] In addition, the mechanisms of transition operational in small-disturbance environments can be changed or bypassed altogether in high-noise environments; these changes in the mechanisms change the parametric trends in transition. Mechanism-based prediction methods must be developed, supported in part with measurements of the mechanisms in quiet wind tunnels.

Development of Quiet-Flow Wind Tunnels

Only in the last two decades have low-noise supersonic wind tunnels been developed.[2,5] This development has been difficult, since the test-

section-wall boundary layers must be kept laminar in order to avoid high levels of eddy-Mach-wave acoustic radiation from the normally-present turbulent boundary layers. A Mach 3.5 tunnel was the first to be successfully developed at NASA Langley.[6] Langley then developed a Mach 6 quiet nozzle, which was used as a starting point for the new Purdue nozzle.[7] Unfortunately, this nozzle was removed from service due to a space conflict; it is now to be reinstalled at Texas A&M. The Purdue Mach-6 tunnel is presently the only operational hypersonic tunnel with any quiet flow, anywhere in the world.

Background of the Boeing/AFOSR Mach-6 Quiet Tunnel

A Mach-4 Ludwieg tube was developed at Purdue from 1992-1994.[8] Quiet flow was achieved at low Reynolds numbers, and the facility was used for development of instrumentation and for measurements of instability waves under quiet-flow conditions. However, the low quiet Reynolds number and the small 4-inch test section imposed severe limitations.

A low-cost hypersonic facility that remains quiet to higher Reynolds numbers is needed. Beginning with Ref. 9, a series of AIAA papers have reported on the design, fabrication and shakedown of this facility, on the development of instrumentation, and on progress towards achieving Mach-6 quiet flow at high Reynolds number.

Ref. 10 summarized these earlier papers, reported on initial quiet flow achieved at low Reynolds numbers with the 6th bleed-slot design, and also on initial measurements with temperature-sensitive paints and hot wires. Ref. 11 reported temperature-sensitive-paints results on the forebody, the results of the 7th bleed-slot throat geometry, and the (minimal) effect of polishing the downstream portion of the Mach-6 nozzle. Ref. 12 reported initial measurements of bypass transition on the nozzle wall, the reduction of low-pressure separation after removing the double-wedge model-support centerbody, and high levels of static-pressure fluctuations in the diffuser when the nozzle-wall boundary layer is laminar, as well as hot-wire and temperature-paints measurements on a sharp cone. Ref. 13 reported more measurements of bypass transition on the nozzle wall, along with the disappointingly minor effect of bypassing the bleed-slot air direct to the vacuum tanks. It also reports more measurements in the diffuser, the first measurements in the contraction entrance, initial measurements of condensation, the successful fabrication of a new sting support, and preliminary hot-wire measurements on cones, along with hot-wire calibrations. Ref. 14 reported uncalibrated measurements of the fluctuations in the contraction entrance, the negligible effect of introducing small controlled disturbances in the driver tube, the helium-sniffer leak tests, initial work towards high-pressure operation and the effect of downstream disturbances from small jets. It also reported temperature effects on the Kulite calibrations, and progress with the hot-wire calibrations and stability measurements. Ref. 15 reported additional measurements in the contraction entrance and measurements downstream of the nozzle.

The Boeing/AFOSR Mach-6 Quiet Tunnel

Quiet facilities require low levels of noise in the inviscid flow entering the nozzle through the throat, and laminar boundary layers on the nozzle walls. To reach these low noise levels, conventional blow-down facilities must be extensively modified. Requirements include a 1 micron particle filter, a highly polished nozzle with bleed slots for the contraction-wall boundary layer, and a large settling chamber with screens and sintered-mesh plates for noise-reduction. To reach these low noise levels in an affordable way, the Purdue facility has been designed as a Ludwieg tube. A Ludwieg tube is a long pipe with a converging-diverging nozzle on the end, from which flow exits into the nozzle, test section, and second throat (Figure 1). A diaphragm is placed downstream of the test section. When the diaphragm bursts, an expansion wave travels upstream through the test section into the driver tube. Since the flow remains quiet after the wave reflects from the contraction, sufficient vacuum can extend the useful runtime to many cycles of expansion-wave reflection, during which the pressure drops quasi-statically.

Two methods are now available to provide flow in the nozzle-throat bleed slots. A fast valve remains connected directly between the bleeds and the vacuum tank, allowing the bleed air to be dumped directly into the tank, with a small but significant delay of about 1/2 sec., which increases to perhaps 2 sec. at very low pressures, when the existing valve does not work well. This is called the “active” bleed system. In addition, the original plumbing connecting the bleed air to the diffuser has been reconnected,

which constitutes the "passive" bleed system. A tee permits the use of either system. The fast valve to the tank has the advantage of eliminating any difficulties associated with the jets of air in the diffuser, but delays the startup of the flow, and does not open well at very low pressures. The direct line to the diffuser allows quick passive timing of the start up, but introduces jets of air into the diffuser. Since recent measurements suggest that these jets are usually not a problem, this simple passive timing system is again desirable.

Figure 2 shows the end of the nozzle with the Pitot probe placed at z=75.3 inches, where z is the distance downstream of the throat. The Pitot probe shows indirectly what is occurring at the boundary layer far upstream. The acoustic origin is the point where noise originates in the boundary layer. This propagates along Mach lines to the center of the tunnel where it is detected by the Pitot probe Kulite pressure transducer.

A Senflex hot film array from Tao of Systems Integration, Inc. is placed in the bottom of the tunnel. Figure 3 shows a diagram of this array, where the flow direction is from top to bottom. The array is attached to a window blank in the last section of the nozzle as shown in Figure 2. The sensors are spaced 1/4 inch axially along the center of the array. Additionally, there are off-center sensors placed in the first, last and center axial locations. The off-center sensors are located 1/2 inch from the centerline of the array.

Using simultaneous data from multiple hot films, it will be possible to see the movement of transition, and may also be possible to find separation points by looking for phase reversal in the signals from the hot films.[16] This allows direct information about what is happening at the tunnel wall and a clearer understanding of the conditions in the boundary layer.

Downstream of the nozzle is a sting support that allows a model to be placed in the tunnel. During testing of the empty tunnel, this is removed when necessary. This sting support is a more streamlined version of the double wedge that was previously used, though it may still be disturbing the flow. Images of the tunnel are available at http://roger.ecn.purdue.edu/~aae519/BAM6QT-Mach-6-tunnel/, along with earlier papers and other documentation.

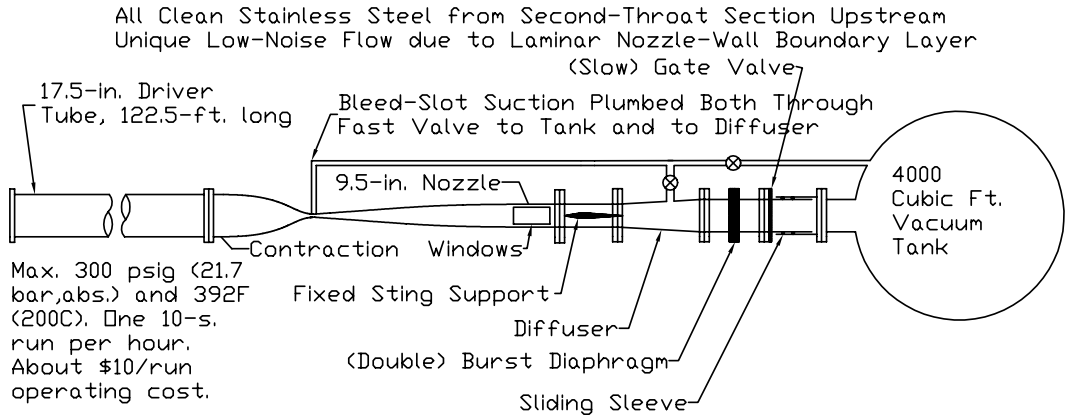

Figure 1: Schematic of Boeing/AFOSR Mach-6 quiet tunnel.

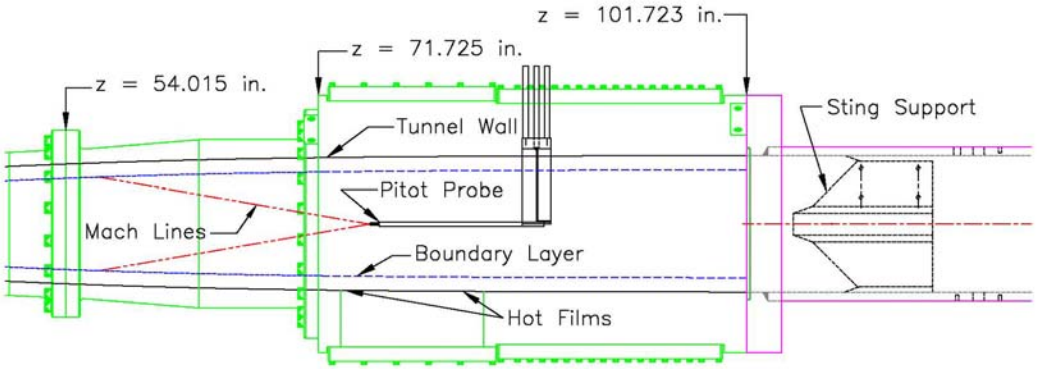

Figure 2: Schematic of the end of the nozzle.

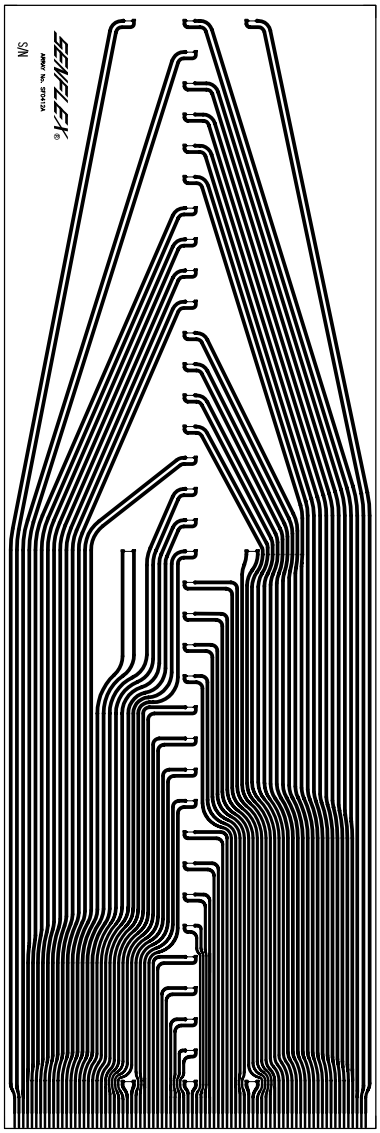

Figure 3: Hot-film array (9x3 inches).

Shock/Boundary Layer Interactions

It is generally assumed in supersonic flow that disturbances can only travel downstream. However, near the wall in the boundary layer, the flow is subsonic, and it is possible for disturbances to be transmitted upstream. In the Mach-6 tunnel, shock/boundary layer interactions occur when shocks impinge on the sidewall of the tunnel. The shocks originate from the sting support or from models placed in the tunnel. These shocks disturb the boundary layer and can separate the flow far upstream.

These kinds of shock/boundary layer interactions are an important problem for hypersonic vehicles. These occur whenever a shock comes in contact with another surface. Examples of this are an impinging shock, a bow shock intersecting a deflected flap, and a glancing shock, where the wing meets the body of the vehicle. For scramjets, the shock structure and boundary layer interactions can become quite complex as shown in Figure 4.

One of the simplest types of shock/ boundary layer interaction is when an oblique shock impinges on a wall. In inviscid flow, there would be a straightforward shock reflection. With a boundary layer, this becomes more complicated as shown in Figure 5 and in the enlarged view in Figure 6. In the boundary layer, the velocity drops so that it reaches the no-slip condition at the wall. Since the Mach number also drops when moving closer to the wall, the oblique shock bends and becomes weaker until it reaches the sonic line in the boundary layer, where it disappears.[17] In the subsonic portion of the boundary layer, information from the pressure rise caused by the shock is sent upstream, allowing a more gradual pressure increase near the wall. This increase in pressure ahead of the place where the shock impinges the boundary layer causes the boundary layer to thicken, or if the shock is strong enough, to separate. The thicker or separated boundary layer causes a shock to emanate from the boundary layer upstream which will interact with the initial oblique shock.

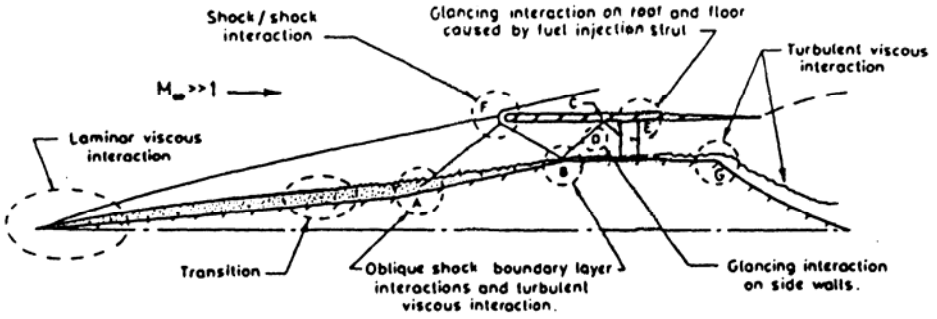

Figure 4: Shock/Boundary-Layer interactions in a scramjet inlet.[18]

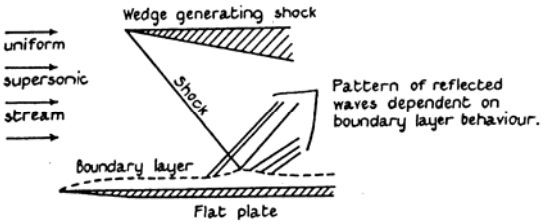

Figure 5: Oblique shock impinging on a boundary layer.[19]

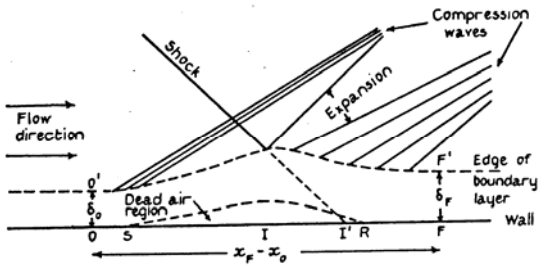

Figure 6: Detail of Boundary Layer where oblique shock impinges.

A turbulent boundary layer has a subsonic region that is much smaller than in a laminar boundary layer. This allows a shock to separate a laminar boundary layer much more easily. To generate comparable separation regions, a shock must be 5-10 times stronger with a turbulent boundary layer than for a laminar boundary layer.

The impinging shock can also have an effect on transition. At very low Reynolds numbers, the boundary layer will be laminar before and after the shock. At a higher Reynolds number, where the flow is near transitional, the flow will be laminar before the shock and separation, but reattach as a turbulent boundary layer.[20] Since the subsonic portion of the boundary layer is thicker for laminar boundary layers, it is also possible that unsteady fluctuations might feed upstream, and cause transition to occur sooner, as observed at NASA Langley Research Center.[21] As this would then generate a turbulent boundary layer with reduced upstream influence, this could be a very unsteady situation.

RECENT INCREASE IN QUIET-FLOW REYNOLDS NUMBER

By adding instrumentation to the nozzle of the Mach 6 Ludwieg Tube, more information regarding the early transition of the nozzle-wall boundary layer could be obtained. However, no access ports for instrumentation were machined into the electroformed nozzle throat, in order to avoid damaging the very low surface-roughness finish. To allow adding instrumentation, a surrogate aluminum nozzle throat was machined to the same specifications as the original. However, this nozzle was only hand-polished by a skilled machinist and thus had a much larger surface roughness than the original nozzle. If this nozzle provided quiet flow to the same stagnation pressure, it could be easily modified to add instrumentation, and data regarding the early nozzle boundary layer transition could be obtained. An image of the surrogate nozzle can be seen in Figure 7.

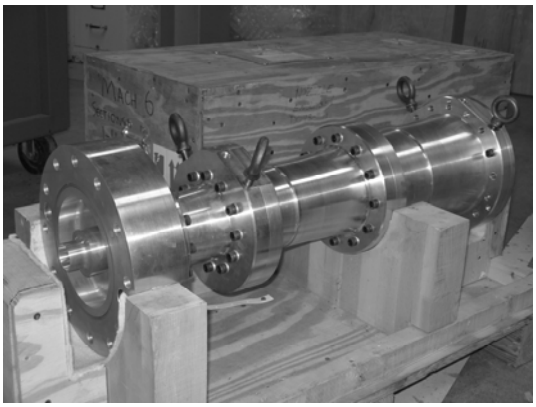

Figure 7: The aluminum surrogate nozzle

The surrogate nozzle was successfully substituted for the original nozzle and was then examined to see what range of quiet flow, if any, was possible. All measurements were recorded on an 8-bit Tektronix TDS7104 digital oscilloscope operating in Hi-Res mode. A Kulite model XCQ-062 pressure transducer was used to measure stagnation pressure on the nozzle centerline at several axial locations. Additionally, a Kulite model XTEL-190-200A pressure transducer was used to measure static pressure at the contraction entrance.

Initially, the Pitot probe was placed at an axial location of 75.3 inches. The nozzle throat is taken to be z=0.0 inches. Tunnel runs were made for initial stagnation pressures of 8.0, 12.0, 14.0, 18.0, 20.0, 21.5, 23.0, 25.0, 27.0, and 29.0 psia at 160ºC using the passive bleed system. The results of these runs can be seen in Figure 8. Percent RMS pressure fluctuations, a measure of tunnel noise levels, is plotted against driver tube pressure. For comparison, data from the original nozzle with the Pitot at the same axial location have been plotted as well. As can be seen, quiet flow was achieved up to stagnation pressures of

almost 20 psia with the surrogate nozzle. This is more than double the 8 psia limit with the original nozzle.

Figure 9 shows a close-up of the noise levels for both nozzles running quietly. As can be seen, the surrogate throat had quiet noise levels between 0.05 and 0.12 percent for the new quiet pressures between 8 and 20 psia. For pressures below 8 psia, where the original throat provides quiet flow as well, the surrogate throat had slightly higher percent noise levels. The difference between the original and surrogate throat noise levels here seems to be negligible. The actual RMS levels (not shown) were nearly identical for the surrogate throat at all quiet pressures. The normalized fluctuations are seen to increase with decreasing pressure due to the decreased signal to noise ratio at lower pressures. The surrogate throat performs very similarly to the original throat for stagnation pressures of 8 psia and below and has much lower noise levels than the original from 8 to 20 psia.

As is seen in Figure 8, the percent RMS fluctuations for the original nozzle increase and then gradually approach the quiet levels with decreasing driver tube pressure. This is evidence of intermittent turbulent spots in the boundary layer as it begins to laminarize. The noise levels for the surrogate nozzle, in sharp contrast, drop off very suddenly with no discernible intermittent zone. The cause of this behavior is currently unknown.

Another curious aspect of the noise levels in the surrogate nozzle is the driver tube pressure at which quiet noise levels are first achieved. It was observed that for decreasing initial driver tube pressure, the pressure at which quiet flow was first observed increased. For instance, for an initial pressure of 27.0 psia, the tunnel first operated quietly at approximately 19.1 psia whereas for an initial pressure of 21.5 psia, quiet flow was observed when the driver tube pressure had dropped to 19.8 psia. This behavior also remains unexplained but suggests a link to the boundary layer development in the driver tube.

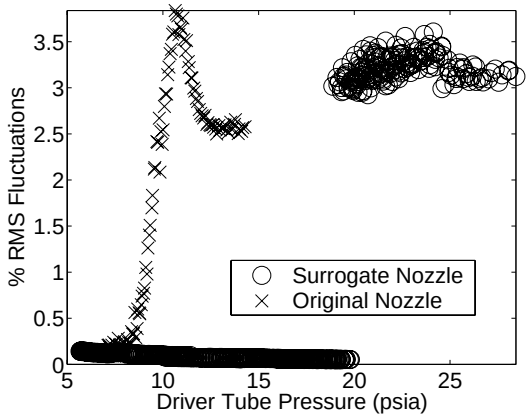

Figure 8: Percent RMS fluctuations for original and surrogate nozzle at z=75.3 inches

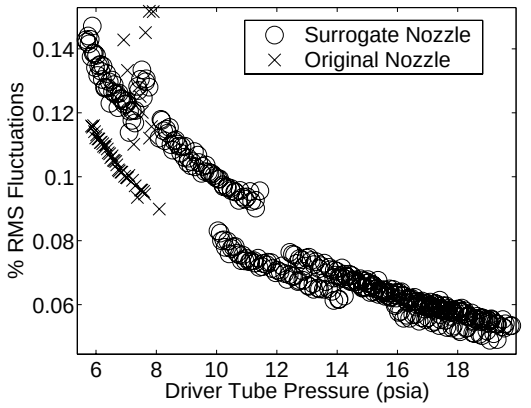

Figure 9: Close-up of noise levels under quiet conditions for both nozzles at z=75.3 inches

If transition in this case were due to linear amplification of instabilities, it was expected that Pitot measurements further upstream in the nozzle would yield quiet flow to higher stagnation pressures. To this end, a long Pitot probe, capable of reaching axial locations much further upstream in the nozzle, was used in place of the original Pitot probe at an axial location of 45.0 inches. Runs were made at initial stagnation pressures of 8.0, 14.5, 20.0, 21.5, 25.0, and 27.0 psia. The Pitot was then moved back to an axial location of 57.0 inches and runs at similar pressures were carried out.

Mach number as a function of driver tube pressure can be seen in Figure 10. As expected, the Mach number at an axial location of 45.0 inches is markedly less than at 57.0 or 75.3 inches due to the nozzle diameter change between the two locations. Curiously, the Mach numbers for axial locations of 57.0 and 75.3 inches are very similar. However, these results

are within previously observed experimental scatter and do not necessarily indicate that the Mach numbers are the same at these different locations.

The Mach number for similar measurements made with the original nozzle throat can be seen in Figure 11. As can be seen, the Mach numbers are very similar for both the original and surrogate nozzle throats. There is a discrepancy for a driver tube pressure of approximately 25 psia at z=45.0 inches. Here, the original nozzle throat's Mach number is markedly less than that of the surrogate. The difference, however, is only slightly more than the scatter between runs at other pressures and axial locations and is not a major point of concern.

Figure 12 shows the percent RMS fluctuations at all three axial Pitot locations for the surrogate nozzle. As can be seen, the pressure at which the tunnel became quiet seems to be independent of axial location. This strongly suggests that normal transition mechanisms are being bypassed and some other phenomenon is responsible for the sudden shift in tunnel noise levels at three axial locations for the same pressure.

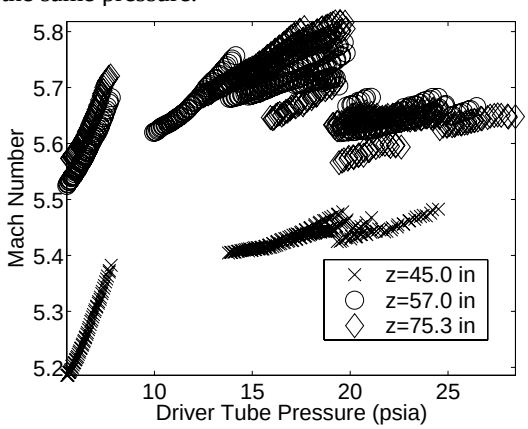

Figure 10: Mach number at three axial Pitot locations for the surrogate nozzle throat

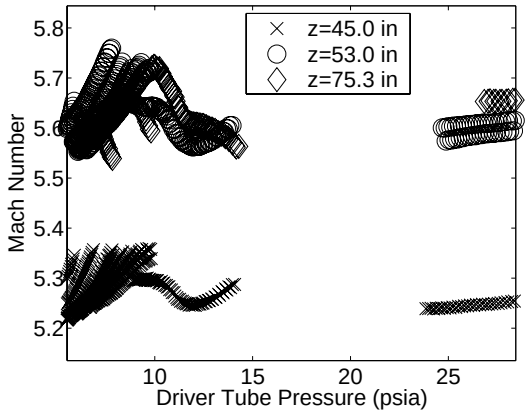

Figure 11: Mach number at three axial locations for the original nozzle throat

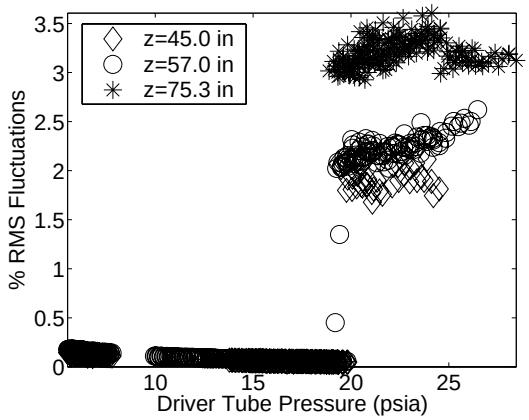

Figure 12: Percent RMS fluctuations at three axial Pitot locations

It is thought that the bypass mechanism responsible for early transition is connected to the contour of the bleed lip. It has been shown that the location and size of a small separation bubble on the main flow side of the bleed lip is very sensitive to small changes in bleed lip geometry.[15,22] Since flaws on the order of 0.001 inches or less had substantial effects on the computed bubble sizes, and since such flaws are on the order of likely machining error, it is thought that some subtle difference exists between the bleed lips of the original and surrogate nozzles causing a larger separation bubble in the original throat than in the surrogate throat. A smaller bubble in the surrogate nozzle throat could allow the nozzle-wall boundary layer to remain laminar to higher stagnation pressures permitting a larger range of quiet flow.

In order to ascertain if this assumption is correct, the surrogate nozzle will be precision measured and polished. It will be tested again to see what effect, if any, the polish has on quiet flow levels. The original nozzle will then be

precision measured. Modifications to the surrogate and/or original nozzle will then be made as CFD computations performed at Rutgers University.

CAUSE OF SEPARATION AT END OF NOZZLE

It has been reported in the past that the flow is separated at the back of the nozzle when there are laminar boundary layers along the nozzle. This was believed to be caused by shocks from the sting mount separating the laminar boundary layer. When the boundary layer is turbulent, no separation is evident, as turbulent boundary layers are more difficult to separate. In order to verify this theory, the sting mount was temporarily removed. The data in this section of the paper is taken with the surrogate nozzle, so the effect of varying pressure can be studied up to 20 psia with laminar boundary layers.

Effect of Sting Mount

Figure 13 compares the Mach number for runs with and without the sting mount with the Pitot probe at z=84.5 inches. The initial driver tube pressures were 8.03 psia for the run with no sting mount and 8.01 psia for the run with the sting mount. Lower Mach numbers indicate a higher Pitot pressure, probably caused by a separation. The case with the sting mount has a large separation that increases throughout the run. The case without the sting mount appears to remain attached at higher pressures. However, an intermittent separation appears to occur later in the run as the driver tube pressure drops. Figure 14 shows the noise levels for the same data. The noise levels are low except when the separation occurs. The separations result in huge noise levels of 30 to 50 percent.

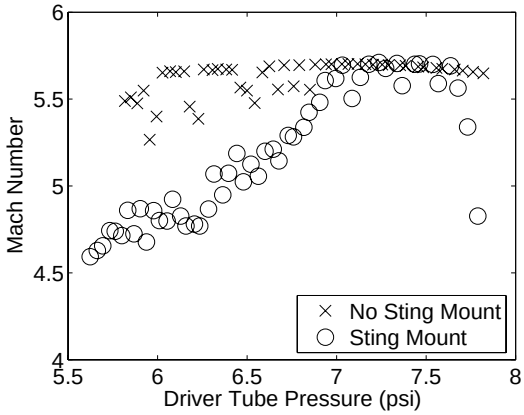

Figure 13: Effect of sting mount on Mach number with Pitot on centerline at z=84.5 inches below 8 psia.

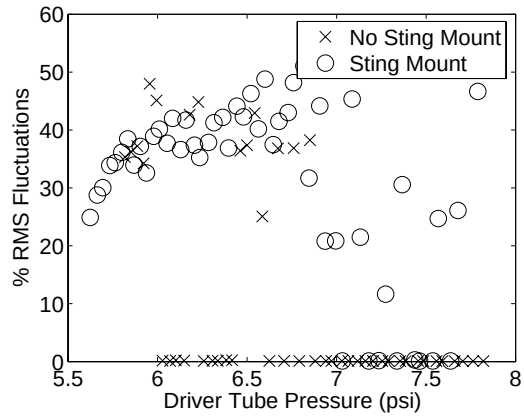

Figure 14: Effect of sting mount on noise with Pitot on centerline at z=84.5 inches below 8 psia.

The effect of the sting mount was also compared at higher driver tube pressures as shown in Figures 15 and 16. The initial driver tube pressures were 19.95 psia for the run with the sting mount and 20.01 psia for the 3 runs with no sting mount. Figure 15 shows that at slightly higher pressures without the sting mount, the separation that is occasionally present at lower pressures is absent. With the sting mount, the separation is still present, but it is less consistent than at lower pressures. The amount of separated flow was not very consistent between the three runs with the sting mount, though separation is present at some point during all three runs. This indicates that the acoustic origin for this probe location is near the furthest forward location that the separation reaches under these conditions. Figure 16 shows the noise levels are again very large when the separation is present.

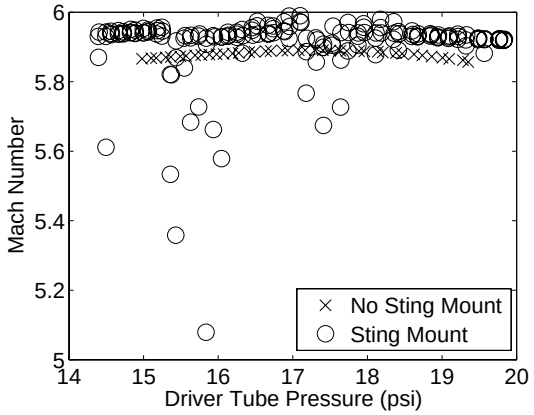

Figure 15: Effect of sting mount on Mach number with Pitot on centerline at z=84.5 inches below 20 psia.

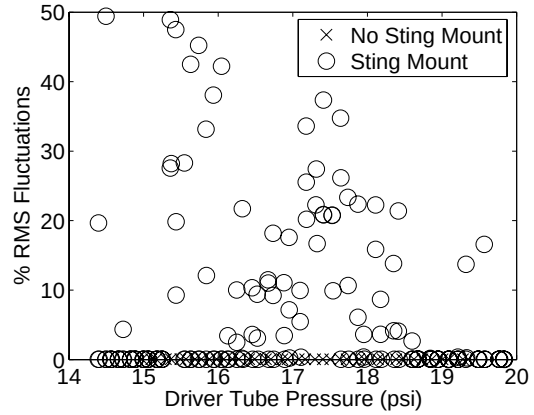

Figure 16: Effect of sting mount on noise with Pitot on centerline at z=84.5 inches below 20 psia.

Separation with Sting Mount Removed

Figure 17 and Figure 18 show the effect of axial location on the separation observed with the sting mount removed. The Pitot probe was placed at z-locations of 75.3, 84.5, and 93.5 inches. The initial driver tube pressure was 8.03 psia for all three runs. The Pitot probe shows flow that is rarely separated at z=75.3 inches, a little more separated at z=84.5 inches, and always separated at z=93.5 inches. It is unknown why the Mach number is lower at z=84.5 inches than it is at z=75.3 inches when no separation is apparent. Figure 18 shows again that the noise levels are extremely high when the unsteady separation occurs. This large noise level ranges from about 20 to 50 percent.

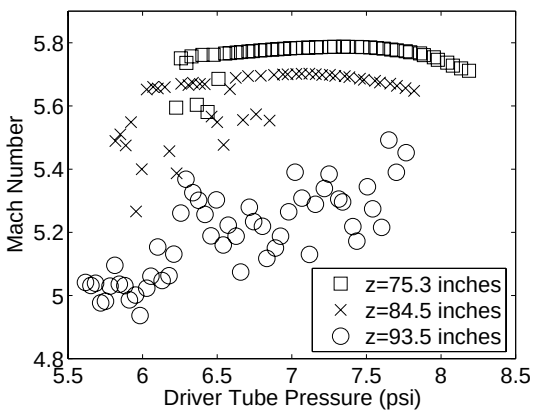

Figure 17: Effect of axial location on Mach number with Pitot at z=84.5 inches below 8 psia.

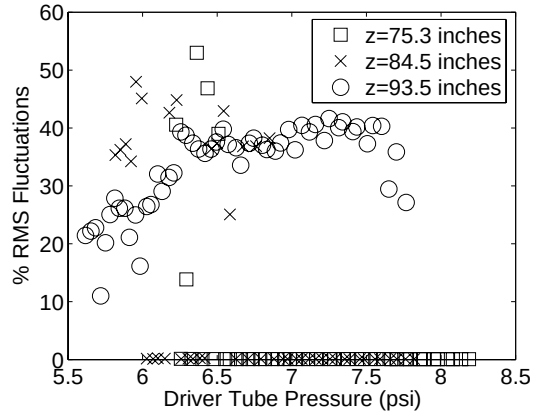

Figure 18: Effect of axial location on noise with Pitot at z=84.5 inches below 8 psia.

Figures 19 and 20 show the effect of axial location on the separation observed with the sting mount removed at higher pressures. This shows that the higher-pressure flow remains attached as far back as can currently be measured with a Pitot probe on the centerline. The noise levels also show quiet flow at all of these axial locations.

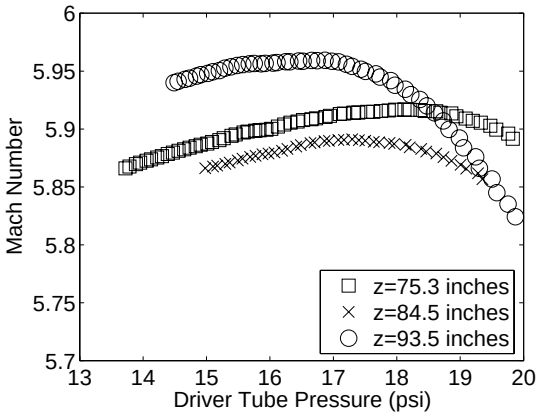

Figure 19: Effect of axial location on Mach number with Pitot at z=84.5 inches below 20 psia.

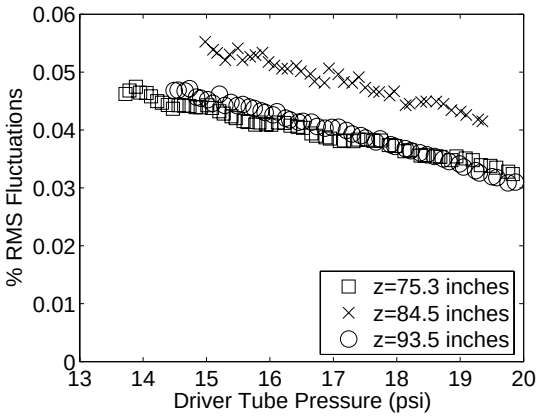

Figure 20: Effect of axial location on noise with Pitot at z=84.5 inches below 20 psia.

Hot Film Measurements Showing Convection Speed of Separations

Measurements with laminar boundary layers and separated flow caused by the sting mount do not cause any fluctuations evident above the electronic noise of the hot films. It is believed that the separation is only evident when the separation front moves over the hot film. With the sting mount in place, the beginning of the separation is always in front of the hot films. Figure 21 contains a section of a run with an initial driver tube pressure of 8.03 psia, showing disturbances with the sting mount removed. The top trace shows the Pitot probe at 93.5 inches and the bottom three traces are from hot films at various axial locations. There are corresponding fluctuations on all sensors at approximately the same times. The hot films show that the fluctuations are largest near the aft sensor and decrease further forward. Some of the smaller fluctuations in the z=80.70 inch trace do not propagate forward to the other hot film locations.

When a single fluctuation is examined more closely, the movement of the separation can be seen in time, as shown in Figure 22. The disturbance appears on the hot film at z=80.70 inches at approximately 0.435 seconds into the run. This disturbance does not show up on the hot film at z=73.45 inches until about 0.438 seconds. This gives a convection speed of the disturbance of about 60 m/sec. Assuming a stagnation pressure of 160 °C and a Mach number of 5.9, the freestream speed of sound is about 150 m/s.

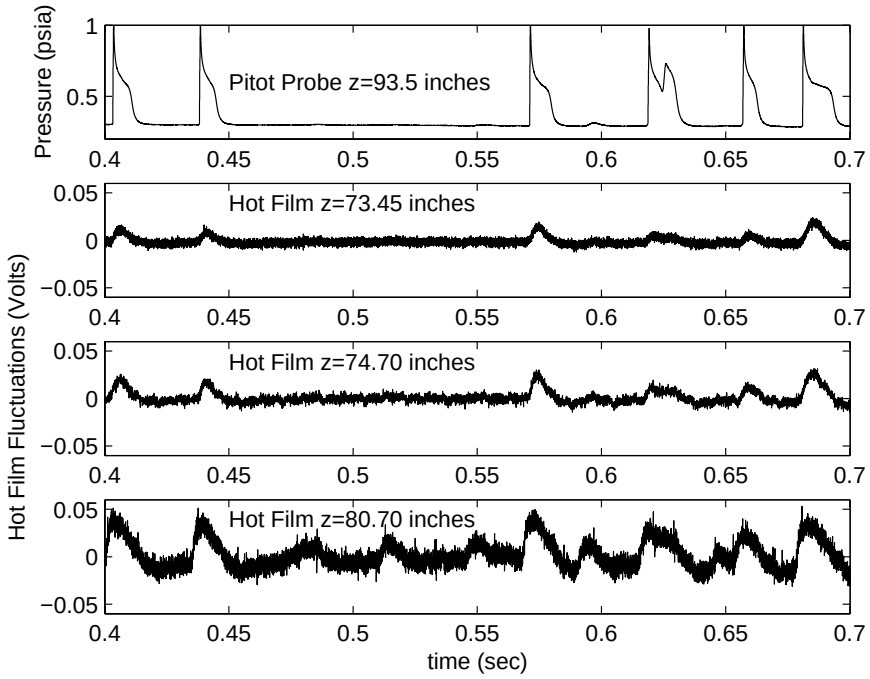

Figure 21: Pitot and hot film data showing unsteady disturbances with no sting mount.

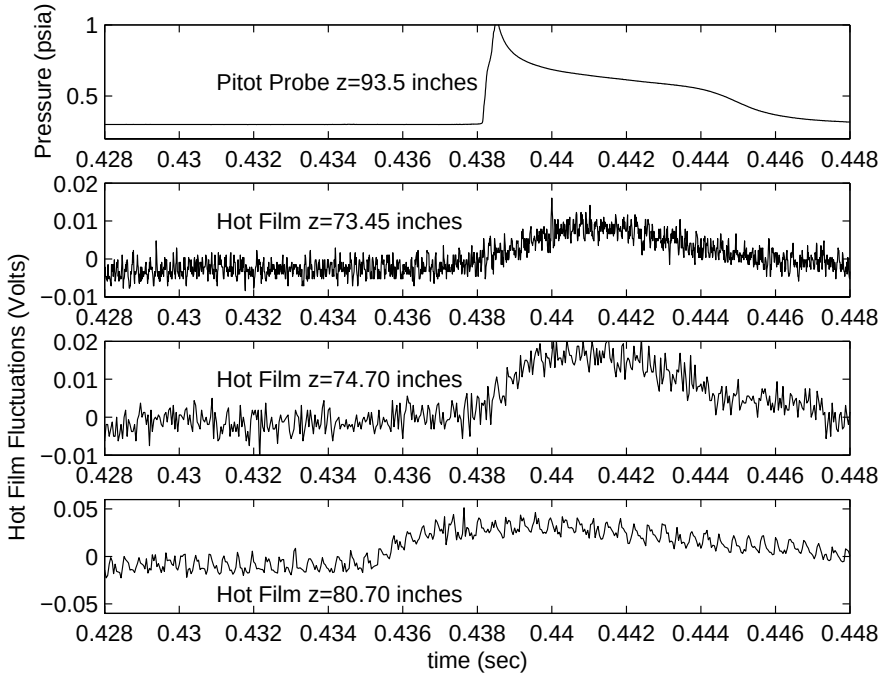

Figure 22: Close-up of unsteady disturbances traveling forward.

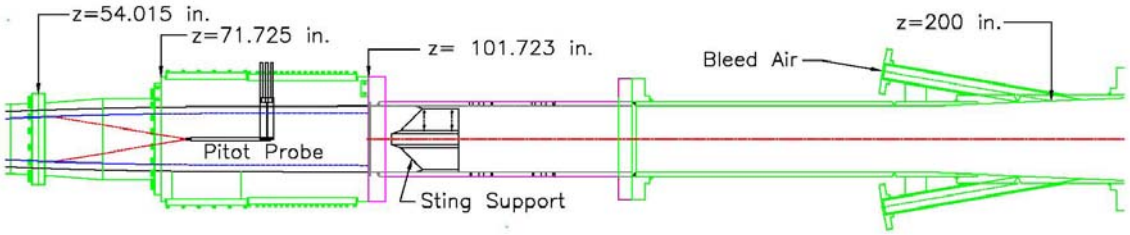

Figure 23: Diagram of end of nozzle and diffuser.

Effect of Jets from Bleeds

Figure 17 shows that when the sting mount is removed, the separation at the end of the nozzle does not extend as far upstream. This indicates that another, lesser disturbance is causing the other separation. Figure 23 shows a diagram of where the bleed air is reintroduced into the diffuser when the passive bleeds are used. The bleed flow can also be directed directly to the vacuum tank, though this requires the use of a fast valve that must be triggered after the start of the run. It was shown previously that disturbances from the jets from the bleed air in the diffuser do not propagate upstream into the nozzle. However, it is possible that with the sting mount removed, the effect of the jets from the passive bleeds can be seen. The passive bleeds, with the jets, are generally used to avoid losing the first 2 seconds of every run. All data shown uses the passive system unless otherwise noted.

The active system was tested to see if the jets from the passive bleeds might be causing the unsteady disturbances. Figure 24 shows the Mach number for the two configurations with the Pitot probe placed at z=93.5 inches. The initial driver tube pressures were 8.03 psia for the passive bleeds, and 8.00 psia for the active bleeds. This shows that the large unsteady separation is not present with the active bleeds. Figure 25 shows the noise levels for the same data. The noise levels are extremely high with the passive bleeds and quiet when the active bleeds are used.

As shown previously, the unsteady separation shows up on the hot film sensors. A hot film at z=73.45 inches is shown in Figure 26. The fluctuations that are present with the passive bleeds and no sting mount do not show up with the separation that occurs with the sting mount. The trace showing the hot film with the active bleeds shows a larger noise level in the first 2 seconds of the run before the bleed system is operating. This is typical of turbulent boundary layers present when the bleeds are closed. After the bleed system starts, this noise falls away and there is no large unsteady separation. All of this indicates that the separation with no sting mount is caused by the disturbances generated by these jets propagating forward over 120 inches.

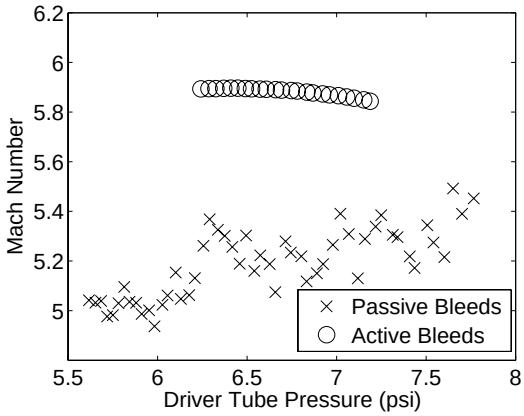

Figure 24: Effect of jets from bleeds on Mach number with Pitot at z=93.5 inches below 8 psia.

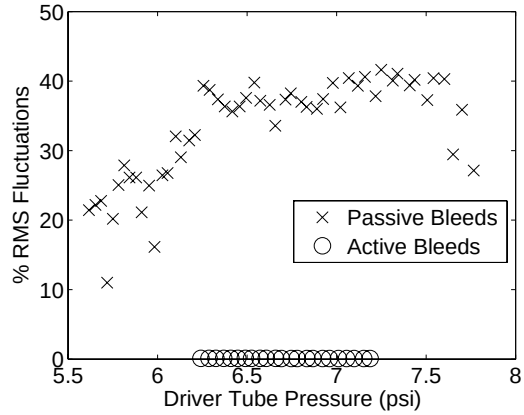

Figure 25: Effect of jets from bleeds on noise with Pitot at z=93.5 inches below 8 psia.

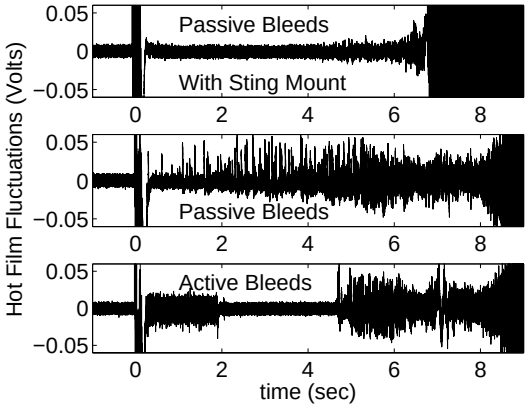

Figure 26: Effect of jets from bleeds shown with hot film at z=73.45 inches.

LAMINAR BOUNDARY LAYER PROFILES

Before the tunnel was tested with the sting mount removed, there was never an unseparated laminar boundary layer that extended to the end of the nozzle where it could be measured. With the sting mount removed, it is now possible to obtain laminar boundary layer profiles. Boundary layer profiles were measured using 2 methods. The Pitot probe is held by a traverse that can be programmed to move throughout the run. This means that each point will be taken at a different time in the run, and a different driver tube pressure, since the driver tube pressure falls during the run. The other method is to move the probe only between runs. This allows points to be compared at the same time after the run start sand at the same driver tube pressure. It was noticed that when the probe was within 0.75 inches of the wall, the hot films stopped showing the unsteady disturbance. This indicates that a shock off of the Pitot probe was disrupting the boundary layer. The Pitot sensor is 0.060 inches, but is held by a tube that expands quickly to 0.3125 inches, and extends back 10 inches. This could be causing some blockage issues.

Figure 27 shows boundary layer profiles where each point was taken with a different run. The initial driver tube pressures were 20.00 psia ± 0.40%. Profiles are shown with data averaged starting at 0.5, 1.3, 2.4, and 3.4 seconds after the start of the run, and following for 0.1 seconds. The average driver tube pressures during these times were, 19.57, 18.61, 17.31, 16.23 psia ± 0.35% respectively. The pressures are nondimensionalized by the freestream Pitot pressure. This shows a laminar boundary layer thickness of about 3/4 inches at z=75.3 inches. It looks like the boundary layer is slightly thicker later in the run than at the beginning, though more points near the edge of the boundary layer would help make this clearer.

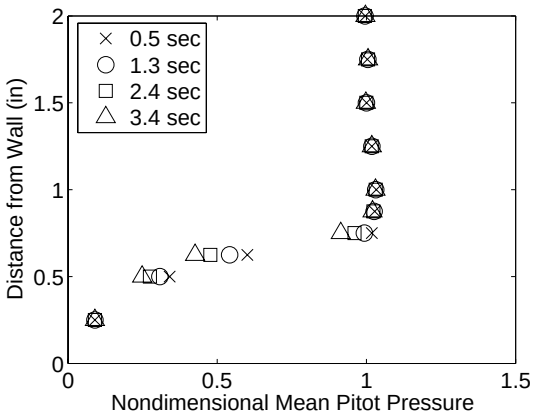

Figure 27: Boundary layer profiles at z=75.3 inches and initial pressure of 20 psia.

Figure 28 shows profiles at three axial locations. Two runs were performed for each profile; one with the probe starting 0.25 inches from the wall, and one with the probe starting 0.375 inches from the wall. The probe then traversed in 0.25 inch increments away from the wall 5 times, and then back toward the wall 4 times. At each location the probe stopped for 0.1 seconds. The mean Pitot pressure is nondimensionalized by stagnation pressure. This figure shows boundary layer thicknesses of slightly less than one inch for the front two locations and about 1 inch for the z=84.5 inches profile.

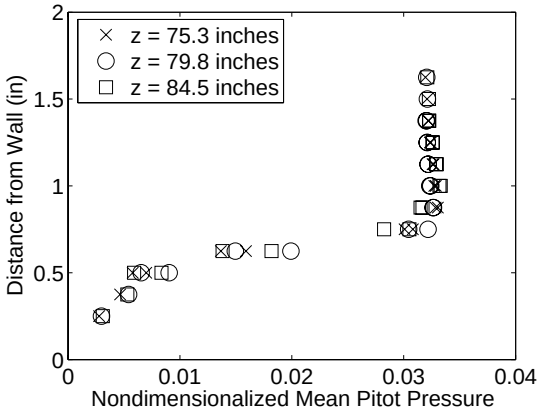

Figure 28: Boundary layer profile at z=75.3 inches and initial pressure of 20 psia using moving traverse.

ATTEMPTS TO PREVENT SEPARATION

Since the sting mount is required to place a model in the tunnel, it is necessary to be able to prevent the separation caused by the sting mount in order to test a model under quiet conditions. Compression rings and a trip ring have been evaluated to try to prevent the disturbances generated by the sting support from propagating upstream when the boundary layer is laminar.

The compression rings consist of an axisymmetric wedge that are placed along the inner wall of the tunnel, as shown in Figure 29. The trip ring consists of a 1/4-inch thick ring that has 18 set screws measuring 1/4"-20. These set screws protrude into the flow at 20 degree intervals around the trip ring. The set screws used varied from 1 inch to 2.5 inches long. The picture of the trip ring in Figure 30 has set screws that are 1.5 inches long.

Figure 31 shows the end of the nozzle with the Pitot probe placed at z=75.3 inches. With an empty sting mount, this shows unseparated laminar flow, at the acoustic origin on the wall somewhere around z=54 inches. This schematic shows a 1 inch maximum-height wedge with a 10 degree wedge angle that is placed just in front of the sting support. Just in front of the compression ring is the trip ring. The set screws shown in this schematic are 1 inch long.

Figure 29: Picture of 0.75 inch maximum thickness compression ring in front of sting mount.

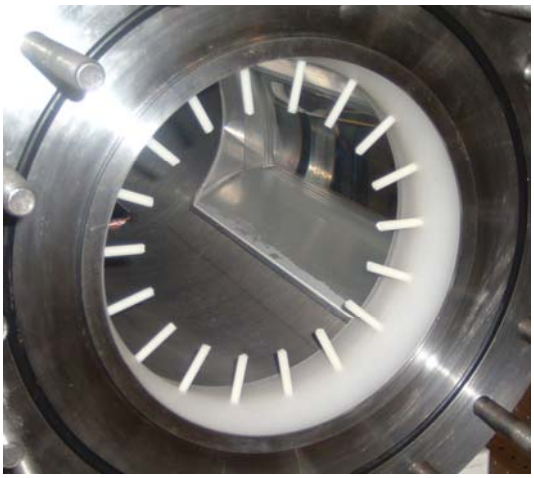

Figure 30: Picture of trip ring with 1.5 inch set screws at end of nozzle.

Figure 32 shows a schematic with the trip ring and no compression ring. In this schematic, the trip ring is drawn with 2.5 inch setscrews. The Pitot probe is shown at z=84.3 inches. At this location, with an empty sting mount, the probe data indicates separated flow, as in Figure 13, indicating that the separation occurs somewhere before a z-location of around 64 inches when traced to the acoustic origin. The location of the acoustic origin is highly speculative as it greatly depends upon the boundary layer thickness.

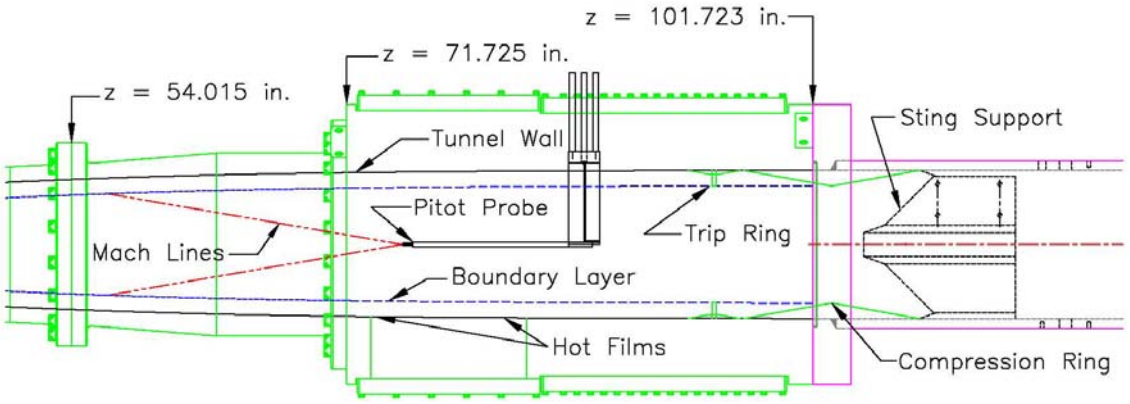

Figure 31: Schematic of the end of the nozzle with a 1 inch compression ring and 1 inch trips.

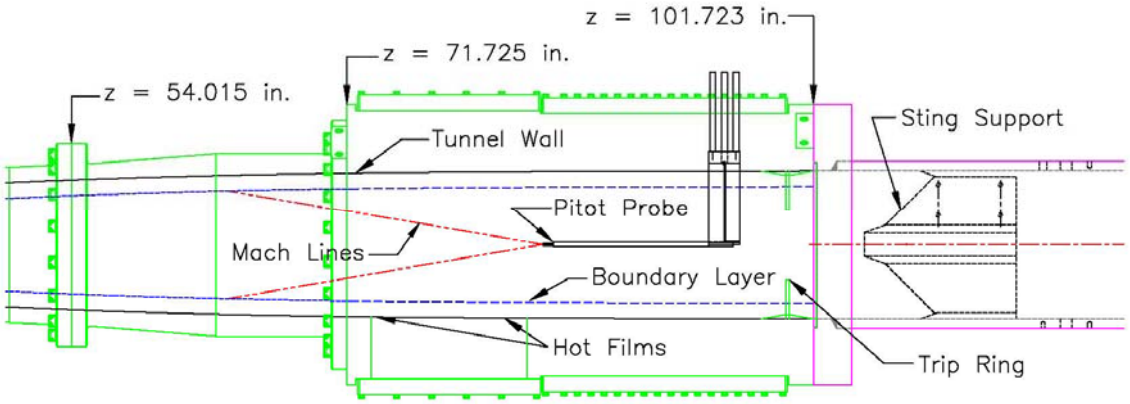

Figure 32: Schematic of the end of the nozzle with 2.5 inch trips.

Results from Compression Rings and Trip Ring

The 1 inch long compression ring with a 10 degree angle was tested both with and without the trip ring directly in front of it. The trip ring used 1 inch set screws. These runs are compared to an empty tunnel, which means no compression ring and no trip ring, in Figure 33 and Figure 34. Figure 33 shows the Mach number from the Pitot probe at z= 75.3 inches. The lower Mach number with the compression ring indicates a separated boundary layer at the acoustic origin at around 54 inches. The empty tunnel is not separated at this location. The trip ring did not seem to have any effect on separation and the compression ring increased the separated region. Figure 34 shows noise levels that are lower for part of the run using the compression ring. This is because the separated flow results in a Pitot pressure 3 times higher than the unseparated flow, and this Pitot pressure is used to nondimensionalize the RMS fluctuations.

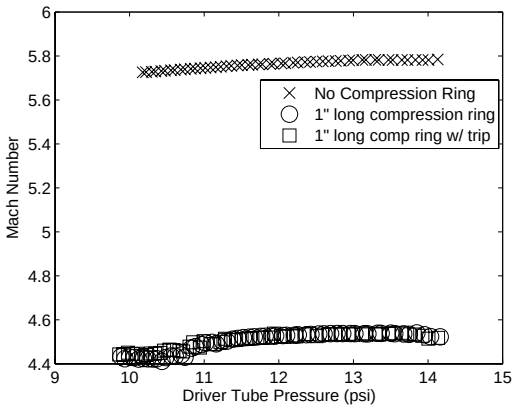

Figure 33: Mach numbers using long 1" compression ring with Pitot probe at z=75.3 inches.

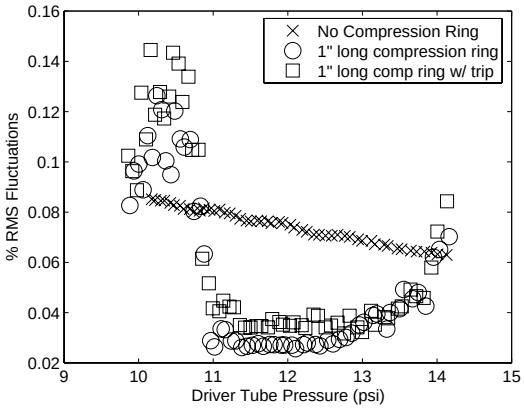

Figure 34: RMS fluctuations using long 1" compression ring with Pitot probe at z=75.3 inches.

A shorter 0.75 inch compression ring was also tested. This has a larger wedge angle of 15 degrees, but less blockage. Figure 35 and Figure 36 show the Mach number and noise for this compression ring with and without trips, and with the trips directly in front of the compression ring and 5.4 inches in front of the compression ring. This shows that this compression ring also increases the separated region, and that the trips have little effect. The noise levels for the separated flows in Figure 36 appear lower because they are being nondimensionalized by a higher Pitot pressure.

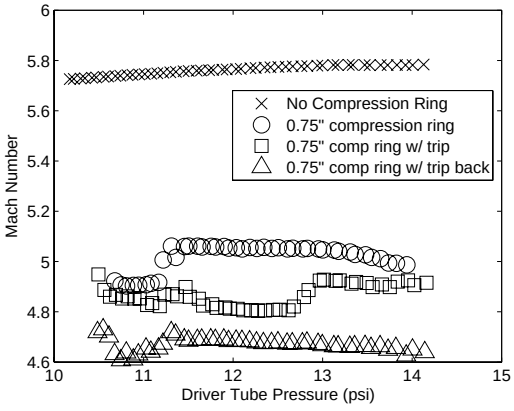

Figure 35: Mach numbers using 0.75" compression ring with Pitot probe at z=75.3 inches.

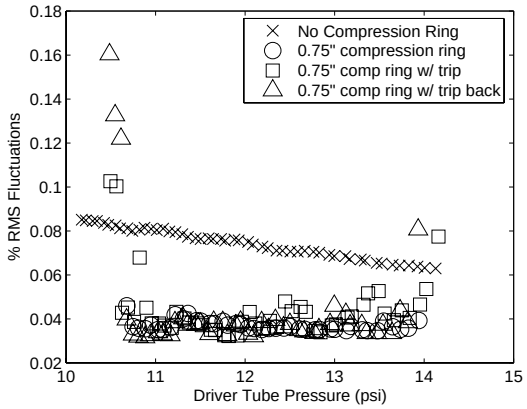

Figure 36: RMS fluctuations using 0.75" compression ring with Pitot probe at z=75.3 inches.

In the runs with the compression rings, the effects of the trip ring were overshadowed by the effects of the compression rings. The trip ring was tested without the compression ring with various trip heights. Figure 37 and Figure 38 show the results for this with the Pitot probe at z= 75.3 inches. Figure 37 shows that the 1.5 inch and 2.5 inch set screws in the trip ring increase the separation at the end of the nozzle. The 1 inch set screws do not have an effect on the Pitot probe data at this location. Figure 38 shows that the 2.5 inch set screws greatly increase the noise level, while the 1.5 inch set screws do not have this effect until very near the end of the run, even though both increase the separation.

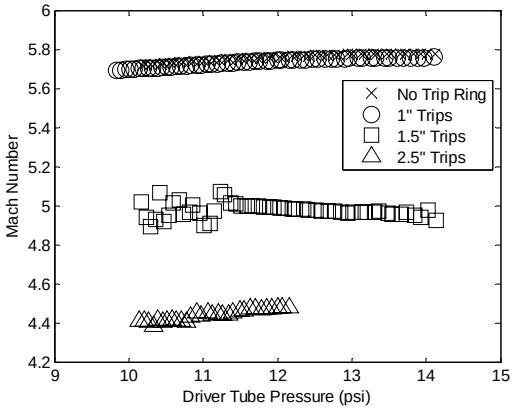

Figure 37: Mach numbers using trip ring with Pitot probe at z=75.3 inches.

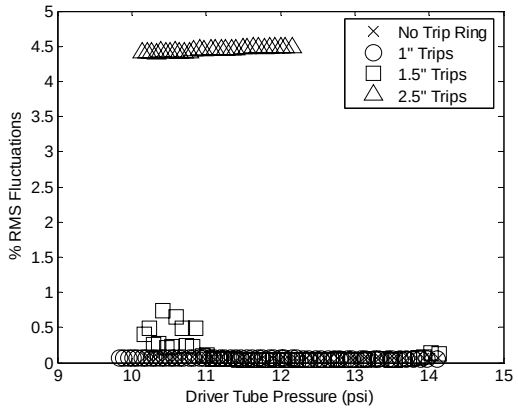

Figure 38: RMS fluctuations using trip ring with Pitot probe at z=75.3 inches.

Trip Effectiveness

After the measurements were conducted showing the ineffectiveness of the trips, a calculation was done of optimal trip size and the distance from trip location to transition using an empirical correlation.[23] This correlation used spherical trips, but should give an indication of what is necessary to trip this flow. The result was unreasonable, requiring spherical trips 4.5 inches in diameter that would cause transition 2 meters downstream of the trip location. As the diameter of the end of the nozzle is only about 9.5 inches, this is not possible. Although the boundary layer present in the tunnel is well outside the range of boundary layers used to develop the correlation, it is possible that this boundary layer is really that difficult to trip.

SUMMARY

The maximum stagnation pressure for quiet-flow in the Mach-6 Ludwieg tube can be maintained has increased from 8 psia to 20 psia utilizing a surrogate nozzle. The most likely cause is a change in small separation bubbles found in computations of the bleed lip flow.

The cause of the separation at the end of the nozzle when laminar boundary layers are present has been found to be the sting mount. Efforts to find a way to prevent the shocks from the sting mount from separating the flow far upstream have met with little success. It may still be possible to eliminate or reduce this separation by moving the sting mount further aft in the diffuser, or by using a different trip ring or compression ring.

When the sting mount is removed, a lesser separation is caused by disturbances from the jets in the diffuser from the passive bleed system propagating forward 120 inches. Using the hot film sensors, the convection speed of these separations can be measured. This separation can be eliminated by eliminating these jets. With all separations eliminated, the first measurements of a laminar boundary layer in the nozzle of this tunnel have been performed.

REFERENCES

1. Steven P. Schneider. Hypersonic laminar-turbulent transition on circular cones and scramjet forebodies. *Progress in Aerospace Sciences*, 40(1-2):1-50, 2004.

2. I.E. Beckwith and C.G. Miller III. Aerothermodynamics and transition in high-speed wind tunnels at NASA Langley. *Annual Review of Fluid Mechanics*, 22:419-439, 1990.

3. Steven P. Schneider. Effects of high-speed tunnel noise on laminar-turbulent transition. *Journal of Spacecraft and Rockets*, 38(3):323-333, May-June 2001.

4. Steven P. Schneider. Flight data for boundary-layer transition at hypersonic and supersonic speeds. *Journal of Spacecraft and Rockets*, 38(1):8-20, 1999.

5. S. P. Wilkinson, S. G. Anders, and F.-J. Chen. Status of Langley quiet flow facility developments. Paper 94-2498, AIAA, June 1994.

6. I. Beckwith, T. Creel, F. Chen, and J. Kendall. Freestream noise and transition measurements on a cone in a Mach-3.5 pilot low-disturbance tunnel. Technical Paper 2180, NASA, September 1983.

7. Alan E. Blanchard, Jason T. Lachowicz, and Stephen P. Wilkinson. NASA Langley Mach 6 quiet wind-tunnel performance. *AIAA Journal*, 35(1):23-28, January 1997.

8. S. P. Schneider and C. E. Haven. Quiet-flow Ludwieg tube for high-speed transition research. AIAA Journal, 33(4):688-693, April 1995.

9. Steven P. Schneider. Design of a Mach-6 quiet-flow wind-tunnel nozzle using the e**N method for transition estimation. Paper 98-0547, AIAA, January 1998.

10. Steven P. Schneider, Shin Matsumura, Shann Rufer, Craig Skoch, and Erick Swanson. Progress in the operation of the Boeing/AFOSR Mach-6 quiet tunnel. Paper 2002-3033, AIAA, June 2002.

11. Steven P. Schneider, Shin Matsumura, Shann Rufer, Craig Skoch, Erick Swanson. Hypersonic stability and transition experiments on blunt cones and a generic scramjet forebody. Paper 2003-1130, AIAA, January 2003.

12. Steven P. Schneider, Craig Skoch, Shann Rufer, and Erick Swanson. Hypersonic transition research in the Boeing/AFOSR mach-6 quiet tunnel. Paper 2003-3450, AIAA, June 2003.

13. Steven P. Schneider, Craig Skoch, Shann Rufer, Erick Swanson, and Matthew Borg. Bypass Transition on the Nozzle Wall of the Boeing/AFOSR Mach-6 Quiet Tunnel. Paper 2004-0250, AIAA, January 2004.

14. Steven P. Schneider, Shann Rufer, Craig Skoch, Erick Swanson, and Matthew P. Borg. Instability and Transition in the Mach-6 Quiet Tunnel. Paper 2004-2247, AIAA, June 2004.

15. Steven P. Schneider, Craig Skoch, Shann Rufer, Erick Swanson, and Matthew P. Borg. Laminar-Turbulent Transition in the Boeing/AFOSR Mach-6 Quiet Tunnel, Paper 2005-0888, AIAA, January, 2005.

16. A. Nakayama, J. P. Stack, J. C. Lin, and W. O. Valarezo. Surface Hot-Film Technique for Measurements of Transition, Separation, and Reattachment Points. Paper 93-2918, AIAA, July 1993.

17. Jean M. Delery. Shock Wave/Turbulent Boundary Layer Interaction and its Control. *Progress in Aerospace Sciences*. Pages 209-279. 1985.

18. J. L. Stollery. Some Viscous Interactions Affecting the Design of Hypersonic Intakes and Nozzles. Advances in Hypersonics: Defining the Hypersonic Environment, Vol. 1. pp. 418-437, 1992.

19. G. E. Gadd. Interactions Between Wholly Laminar or Wholly Turbulent Boundary Layers and Shock Wave Strong Enough to Cause Separation. *Journal of the Aeronautical Sciences*. Vol. 20, No. 11. November, 1953, pp. 729-39.

20. Jean M. Delery. Physcial Features of Shock Wave/Boundary Layer Interaction in Hypersonic Flows. AGARD Conference on Future Aerospace Technology in the Service of the Alliance. April 1997.

21. Steve Wilkinson, Private Communication, 2003.

22. Doyle D. Knight, Private Communication, Feb 2005.

23. E. L. Morrisette, D. R. Stone, and A. H. Whitehead, Jr. Boundary-Layer Tripping with Emphasis on Hypersonic Flows. Viscous Drag Reduction, Plenum Press, New York, 1969, pp. 33-51